The Astrophysical Journal, 849:51 (14pp), 2017 November 1 https://doi.org/10.3847/1538-4357/aa8f45

In Search of Cool Flow Accretion onto Galaxies: Where Does the Disk Gas End?

Joss Bland-Hawthorn[1,2], Philip R. Maloney[3], Alex Stephens[1], Anna Zovaro[1], and Attila Popping[4]
[1] Sydney Institute for Astronomy, School of Physics A28, University of Sydney, NSW 2006, Australia
[2] ARC Centre of Excellence for All Sky Astrophysics in 3 Dimensions (ASTRO-3D), Australia
[3] Centre for Astrophysics and Space Astronomy, University of Colorado, Boulder, CO 80309-0389, USA
[4] Centre of Excellence for All-sky Astrophysics, International Centre for Radio Astronomy Research, 7 Fairway, University of Western Australia, Crawley, Perth, WA 6009, Australia
Received 2017 March 2; revised 2017 September 15; accepted 2017 September 24; published 2017 October 30

Abstract

The processes taking place in the outermost reaches of spiral disks (the "protodisk") are intimately connected to the build-up of mass and angular momentum in galaxies. The thinness of spiral disks suggests that the activity is mostly quiescent, and presumably this region is fed by cool flows coming into the halo from the intergalactic medium. While there is abundant evidence for the presence of a circumgalactic medium around disk galaxies as traced by quasar absorption lines, it has been very difficult to connect this material to the outer gas disk. This has been a very difficult transition region to explore because baryon tracers are hard to observe. In particular, H I disks have been argued to truncate at a critical column density ($N_{\rm H} \gtrsim 10^{19.5}\,{\rm cm}^{-2}$ at 30 kpc for an $L_\star$ galaxy) where the gas is vulnerable to the external ionizing background. But new, deep observations of nearby $L_\star$ spirals (e.g., Milky Way, NGC 2997) suggest that H I disks may extend much farther than recognized to date, up to 60 kpc at $N_{\rm H} \approx 10^{18}$ cm^{-2}. Motivated by these observations, here we show that a clumpy outer disk of dense clouds or cloudlets is potentially detectable to much larger radii and lower H I column densities than previously discussed. This extended protodisk component is likely to explain some of the Mg II forest seen in quasar spectra as judged from absorption-line column densities and kinematics. We fully anticipate that the armada of new radio facilities and planned H I surveys coming on line will detect this extreme outer disk (scree) material. We also propose a variant on the successful "Dragonfly" technique to go after the very weak Hα signals expected in the protodisk region.

Key words: galaxies: evolution – galaxies: individual (NGC 2997, NGC 3198) – Galaxy: disk – intergalactic medium – local interstellar matter

1. Introduction

The details of how gas gets into galaxies remain something of a mystery. Does it come in hot or cold, with or without dark matter, in a mildly coherent or a highly turbulent process, at a constant rate or in a stochastic fashion, and so on. The answers are intimately connected to how galaxies form and evolve over cosmic time, and how baryons work with dark matter to build up angular momentum over billions of years. The slow progress in understanding accretion is due to the difficulty of observing gas in the outer reaches of galaxies. The hot, warm, and cold phases are all hard to observe directly in most galaxies beyond the extent of the visible disk or halo.

Over the past decade, a theoretical picture has emerged where gas accreting into galaxies is thermally and dynamically cold below a critical halo mass threshold ($\sim 10^{12}\,M_\odot$), while more massive systems are fed by relatively hot gas (e.g., Birnboim & Dekel 2003; Kereš et al. 2005, 2009). Most of this activity occurred at $z = 1$–5, although accretion is ongoing at a lower level for perhaps one-half of all galaxies to the present day, including our own Milky Way. Building on these ideas, the *Horizon-AGN* simulations present a picture where mass and angular momentum build-up in galaxies is a highly coherent process (e.g., Dubois et al. 2014; Codis et al. 2015). The flow of gas down filaments with velocity $\boldsymbol{v}$ leads to a net vorticity $\boldsymbol{\omega}$ ($=\nabla \times \boldsymbol{v}$) that assists the build-up of angular momentum during collapse. Depending on the impact parameter of the infalling gas, the vorticity arises partly from oblique shocks as the gas gravitates toward and along the dark-matter-dominated filaments. The derived vorticity today[5] ($\omega \approx 100$ km s^{-1} Mpc^{-1}) is considerably larger than what is generated in a turbulent accretion process (e.g., Cornuault et al. 2016).

The extent of the outer gas disk. Observational evidence for the cool flow scenario is suggestive but indirectly inferred for the most part, for example, from statistical studies of QSO absorption lines. Cool gas traced by Lyα absorption has been detected ubiquitously around galaxies, indicating the presence of a circumgalactic medium (CGM) out to 150 kpc in passive and star-forming galaxies (e.g., Tumlinson et al. 2013). The mass of the CGM can be comparable to or exceed the stellar mass (Faerman et al. 2017), and the strength of the Lyα absorption increases toward the center of the galaxy (see Borthakur et al. 2016). But are we seeing halo gas, a disk–halo transition region, or cooling material settling into an outer "protodisk"? The answer is unclear, although statistical evidence is emerging of a rotating torus-like region in the outermost parts of disk galaxies (see Ho et al. 2017).

The most direct probe of the atomic hydrogen that typically dominates the outer disks of $z = 0$ spiral galaxies is the 21 cm H I emission line. Until recently, the deepest H I observations have rarely dipped below $N_{\rm H} \approx 10^{19.3}\,{\rm cm}^{-2}$ at 5σ in a narrow velocity channel (e.g., Westmeier et al. 2013). In an important unpublished experiment (see van Gorkom 1991), van Albada et al. observed the isolated spiral galaxy NGC 3198 for 100 hr with the VLA in order to reach a column density sensitivity of $N_{\rm H} \approx 4 \times 10^{18}\,{\rm cm}^{-2}$, with the expectation of probing the H I

[5] The size of the vorticity is likely to scale inversely as $(1 + z)$ and was therefore weaker in the past.

emission to beyond $R \sim 60$ kpc. To their surprise,[6] the 5×10^{19} cm^{-2} and 4×10^{18} cm^{-2} contours were coincident within their 1′ beam (2.7 kpc for an assumed distance of 9.4 Mpc, but see below).

The impact of a cosmic ionizing background (CIB). Our interpretation of "cool" gas in the extreme outer regions of galaxies is complicated by the highly uncertain (and controversial) CIB. Following earlier discussions of the influence of the CIB on neutral hydrogen in galaxy disks (Felton & Bergeron 1969; Sunyaev 1969; Bochkarev & Sunyaev 1977), Maloney (1993) showed that there should be a critical column density N_c in H I disks at which the gas would go from largely neutral to largely ionized, that N_c would not depend strongly on either the galaxy parameters or the intensity of the ionizing background, and that this transition could plausibly explain the H I truncation observed in NGC 3198, provided the CIB is of order $\phi_i \sim 10^4$ phot cm^{-2} s^{-1}.

This idea was subsequently discussed by many authors with somewhat inconclusive results (Corbelli & Salpeter 1993; Bland-Hawthorn et al. 1997; Walsh et al. 1997; Madsen et al. 2001; Christlein et al. 2010; Adams et al. 2011; Abramova 2012), and the observational situation in particular has not advanced significantly, largely because of the difficulty of achieving such sensitivity and the requisite dynamic range. But H I has now been observed down to $N_{\rm H} \approx 10^{18}$ cm^{-2}, revealing partial bridges, discrete clouds, and extended gas disks around nearby disk galaxies in loose groups (Braun & Thilker 2004; Westmeier et al. 2005; Wolfe et al. 2013, 2016; Pisano 2014). Of particular note, Pisano (2014) used the Green Bank Telescope (GBT) to reach down to $N_{\rm H} \approx 1.2 \times 10^{18}$ cm^{-2} (5σ) in two disk galaxies, NGC 6946 and NGC 2997. Although the single-dish GBT has a large beam (a width of 16 and 32 kpc at the distance of NGC 6946 and NGC 2997, respectively), it does not suffer from the spatial filtering of interferometer observations that makes them insensitive to emission on large angular scales. NGC 6946 was found to have a previously undetected filament connecting it to its companion galaxies, while NGC 2997 exhibited an extended H I disk with an outer radius $R \approx 53$ kpc. By analogy with the outer H I disk simulations of Popping et al. (2009), Pisano suggested the compact filament could be part of a cool, coherent flow (although a tidal interaction origin is also plausible). These papers have inspired our new calculations because the prospect of an extreme outer disk as a generic feature of most galaxies has major implications for understanding how gas gets into disk galaxies.

Inferring the cosmic ionizing intensity. We briefly review the broad range of estimates for the CIB intensity to emphasize that its value is highly uncertain. The present-day background ionizing intensity depends on environment and cosmic evolution (Ćirković et al. 1999; Maloney & Bland-Hawthorn 1999, 2001; Haardt & Madau 2012). Both of these contributions are only crudely constrained at the present time. Weymann et al. (2001) set a 2σ upper limit of 8 mR[7] for the Hα intensity of an opaque cloud illuminated by the CIB, although the uncertainties are dominated by the sky subtraction and the uncertain geometry of the cloud. Compared to the value from Maloney (1993) of $J_o = 4 \times 10^{-23}$ erg cm^{-2} s^{-1} Hz^{-1} sr^{-1}, and the $J = 0.7J_o$ value adopted by Dove & Shull (1994), this is equivalent to an intensity at the Lyman limit of $J = 0.4J_o$. The theoretical estimate of the present-day background of Haardt & Madau (2012) is about a factor of two below this upper limit ($J = 0.2J_o$).

In terms of the H ionization rate, the CIB intensity favored by Maloney (1993) corresponds to $\Gamma_{\rm H} \approx 10^{-13}$ s^{-1}, while the $z = 0$ prediction of Madau & Haardt (2015) is $\Gamma_{\rm H} = 2.3 \times 10^{-14}$ s^{-1} (see Figure 11 of Fumagalli et al. 2017). However, a number of papers on the low-redshift Lyα forest argued that their number was too small by a factor of a few (Kollmeier et al. 2014; Khaire & Srianand 2015; Shull et al. 2015; Viel et al. 2017), and the revised model of Madau & Haardt (2015), updated with new quasar emissivities, predicts a $z = 0$ ionization rate of $\Gamma_{\rm H} \simeq 6 \times 10^{-14}$ s^{-1}.

Very recently, Fumagalli et al. (2017) have claimed detection of CIB-induced Hα fluorescence from the edge of the H I disk of the edge-on spiral NGC 7321. Performing photoionization modeling of the disk,[8] they arrive at a H ionization rate $\Gamma_{\rm H} \sim$ (6–8) $\times 10^{-14}$ s^{-1}, which is in good agreement with the theoretical and low-z Lyα forest-derived numbers discussed above. It is, however, in considerable disagreement with the upper limit (and subsequent claimed 7σ detection[9]) of Adams et al. (2011), which they report as $\Gamma_{\rm H} = 2.0 \times 10^{-14}$ s^{-1} for the same galaxy, even though the Adams et al. (2011) upper limit to the Hα surface brightness is fully consistent with the detection of Fumagalli et al. (2017). This should be taken as an indication of the importance of careful photoionization modeling in extracting ϕ_i from the Hα observations, and that caution should be exercised in accepting any particular value at present; as with Weymann et al. (2001), the uncertainty in the Fumagalli detection is largely systematic.

The main goals of our study. So how are we to understand the well-established existence of gas clouds—even down to $N_{\rm H} \sim 10^{17}$ cm^{-2} (Wolfe et al. 2016)—far beyond the confines of the opaque disk? Can we detect these clouds directly in future deep H I and Hα studies? Do H I truncations even exist at all? These are the main questions addressed by this study.

If an extended (clumpy) component can be revealed as a common feature of disk galaxies, we may be seeing the domain of the protodisk fed by cooling flows seen in some simulations (e.g., Stewart et al. 2011). We are led to revisit the key work of Maloney (1993) and the corroborative study of Dove & Shull (1994), which we extend to the case of a clumpy medium. Given the uncertainty, we consider a broad (factor of 10) range in the value of ϕ_i to cover the highest and lowest estimates of the present-day intensity of the CIB and to facilitate comparisons with earlier work. Note, however, that the critical column N_c only depends on the square root of the extragalactic ionizing flux (see below). As we show, present-day gas disks can in principle extend a factor of two beyond the radial limit at $N_{\rm H} \approx 10^{19.3}$ cm^{-2} of earlier work, and may be detectable to these outer limits with new facilities under development.

The structure of the paper is as follows. In Section 2, we briefly recapitulate the major assumptions and results of Maloney (1993), and we discuss what this model does and does not imply for H I distributions in disk galaxies, as there

[6] They would have been less surprised if the prescient paper of Bochkarev & Sunyaev (1977) had not been unjustly overlooked.

[7] Note that 1 milli-Rayleigh (mR) is defined as $10^3/4\pi$ Hα phot cm^{-2} s^{-1} sr^{-1} equivalent to 5.7×10^{-21} erg cm^{-2} s^{-1} arcsec^{-2} for an unresolved emission line.

[8] As in Maloney (1993), they assume a smooth distribution for the gas, and although they solve for the thermal as well as ionization structure of the gas, the gas scale height z_g is independent of the temperature, although they vary z_g from an initial guess to match the H I and Hα observations.

[9] See http://iactalks.iac.es/talks/view/393.

has been some confusion in the literature on this point. In Section 3, we discuss our galaxy model in detail before describing the computational method in Section 4. The results of the calculations are discussed in Section 5. In Section 6, we look forward to what will be possible in the next few years. At many scale lengths beyond the optical edge, disk stars are rarely observed, and this may conceivably be the domain of the coherent cold flow. But mapping these structures over large areas will require a different observational approach and large amounts of dedicated telescope time, as we discuss. In Section 7, we examine the broader implications of our work.

2. The Critical Column Density and Disk H I Edges

There are only limited theoretical studies that directly or indirectly infer the maximum radial extent of H I in disk galaxies from first principles, that is, in the absence of ionizing radiation. Numerical simulations of $L_\star$ galaxies make a case for H I settling into a disk out to at least 100 kpc in radius (Kereš & Hernquist 2009; Stewart et al. 2011; Nuza et al. 2014), but these are often complex filamentary structures.

Simple arguments can be made that an exponential H I disk is a consequence of cooling in a spinning hot halo (Fall & Efstathiou 1980, Mo et al. 1998). In support of this picture, the hot coronae ($\sim 10^6$ K) of several nearby high-mass disk galaxies have been detected through either stacking or radial binning of a direct X-ray image (Anderson & Bregman 2011; Dai et al. 2012; Miller & Bregman 2013). A disk condensing out of the hot halo can extend to a significant fraction of a virial radius if the hot halo has sufficient angular momentum. In these models, the start time for accretion moves outward from the center, and the accretion timescale increases as a function of the galactic radius. Using this approach, Tepper-Garcia & Bland-Hawthorn (2017) produce a dynamically stable model of the Galaxy in line with the observed halo emissivity constraints. The atomic hydrogen disk has a scale length of $r_d \approx 7$ kpc and $N_{\rm H} \approx 3 \times 10^{17}\,{\rm cm}^{-2}$ at a radius of $r = 80$ kpc. This is the nonionized hydrogen profile we adopt in this work, which is broadly consistent with the observed H I profile in the Galaxy (see below; Kalberla & Dedes 2008).

Independent of any detailed modeling, Maloney (1993) showed that the truncation radius at which H I is observed can be much less than the outer boundary of the gas disk. He presented a simple argument for the critical atomic hydrogen column density in a galactic disk, to which the gas goes from largely neutral to largely ionized, by equating the incident ionizing photon flux to the total column recombination rate within the vertical gas layer. This results in the expression

$$N_c = 2\pi^{1/4}\left(\frac{\phi_i\, z_g}{\alpha_{\rm rec}}\right)^{1/2}, \qquad (1)$$

where z_g is the scale height of the gas and $\alpha_{\rm rec}$ is the recombination coefficient. This can be put into a more useful form by relating z_g to the galactic mass parameters, with the result (see Maloney 1993 for details)

$$N_c \approx 2.6 \times 10^{19}\left(\frac{\phi_{i,4}\sigma_{g,10}V_{150}}{\Sigma_{h,100}}\right)^{1/2}\,{\rm cm}^{-2}, \qquad (2)$$

where $\phi_i = 10^4\phi_{i,4}$ phot cm^{-2} s^{-1}, the gas vertical velocity dispersion is $\sigma_g = 10\sigma_{g,10}$ km s^{-1}, the asymptotic value of the disk rotation velocity $V = 150\ V_{150}$ km s^{-1}, and the halo mass surface density (which is a function of radius) $\Sigma_h = 100\Sigma_{h,100}$ $M_\odot$ pc^{-2}. This analytic estimate was shown to agree very well with the detailed photoionization model results.[10]

The most important assumptions about the atomic gas that go into this calculation are that it is warm and smoothly distributed in the galactic potential; α_B evaluated at $T = 10^4$ K has been used for the recombination coefficient. Because V and the magnitude of Σ_h are tightly related, the ratio of these quantities does not vary strongly from galaxy to galaxy or within galaxies over the radii of interest. The vertical velocity dispersion is typically $\sigma_g = 6$–10 km s^{-1} for the bulk of the H I observed in face-on disk galaxies and independent of radius in the outer disks; this is also comparable to the expected magnitude of σ_g for gas in the warm, neutral phase (but see the discussion below).

What does the existence of such a critical column density imply for galactic H I disks? Notice that this is predicted to be a generic feature of H I disks, provided the assumptions about the gas distribution hold, and that N_c is not strongly dependent on either ϕ_i or the galaxy parameters. Note also that even if the (lower) Haardt & Madau (2012) CIB intensity is correct, N_c will drop by only about a factor of two. For NGC 3198, Maloney (1993) argued that the observed truncation could be explained by photoionization, provided that the total hydrogen column continued to fall as extrapolated from the inner part of the disk (where the total and neutral hydrogen columns are nearly identical). Although reportedly the truncation in NGC 3198 is independent of azimuth (ruling out a warp, for example, as an explanation), only the major axis cut was available for analysis. There are noticeable differences in H I extent between the northeast and southwest sides of the disk, with the southwest being more extended. However, such asymmetries are not really surprising, due to the long dynamical timescales at these radii: the orbital period for gas at 30 kpc in NGC 3198 is more than 10^9 years. The Milky Way's H I distribution, for example, is noticeably asymmetric, with more gas in the south than in the north (Kalberla & Dedes 2008). The observed neutral hydrogen distribution along the two sides of the major axis was reproduced with a model in which the deviations on the two sides from the same exponential falloff in total H were less than 50%.

Hence the moderate asymmetry between the northeast and southwest major axis cuts is not really an issue for the photoionization model. However, it does illustrate an important point: even if all of the model assumptions are satisfied, whether photoionization by the CIB results in a sharp truncation of the disk depends on the shape of the underlying total hydrogen distribution. If this exhibits asymmetries or a change in behavior with increasing radius, this will be reflected in the observed H I distribution. A gas disk with a shallow radial profile can exhibit an extended H I disk even if the column density has dropped below the critical column.

If the assumptions about the nature of the gas distribution are violated, however, then the results can be very different. For example, in a deep H I observation of the edge-on spiral NGC 891 (which has a noticeably lopsided H I distribution between the two sides), Oosterloo et al. (2007) found that the radial extent of the gas increased very little from earlier studies, but

[10] For the numerical results, the critical column was defined as the column where the neutral fraction dropped to 10%. However, since the neutral fraction varies very rapidly around N_c, the precise definition of the neutral-to-total ratio for the numerical N_c is not crucial.

discovered a low-column-density component that extended to large distances above the plane; they argued that this was evidence against the CIB photoionization model for the radial edges of the H I disk, which were likely to be physical edges. We note simply that (1) this is very plausible, but (2) the presence of gas at such large heights above the plane indicates physical conditions very different from those required for the models of Maloney (1993) to apply, for example, the presence of a galactic fountain, in which case the high-altitude atomic hydrogen is almost certainly cooling and condensing and unevenly distributed in a very clumpy medium. In addition, the H I disk of NGC 891 is much less extended compared to the optical disk than that of NGC 3198: on the northern side of the disk, it only extends about 4.5 optical scale lengths, while for the southern side it is about 6 scale lengths. Hence it is more likely that the H I distribution in NGC 891 has been disturbed by stellar processes; the very extended H I disk of NGC 3198 (more than 11 disk scale lengths) is precisely why it was chosen by van Albada et al. for their deep imaging experiment.

Similarly, Kalberla & Dedes (2008) in their study of the Milky Way's H I emission found that gas extended to $R \sim 60$ kpc at low column densities, and they argued that this was inconsistent with the results of Maloney (1993). However, the fit to their H I data shows an abrupt shallowing of the radial distribution beyond 35 kpc, and the vertical velocity dispersion required to explain the vertical extent is 74 km s^{-1}. Whatever the physical mechanism responsible for this distribution, it is unavoidable that this gas is highly clumped, as the velocity dispersion cannot possibly represent thermal motion (WNM).

The distribution and structure of the gas in the outer disks of galaxies are a complicated subject in which many uncertainties remain. The 21 cm H I emission–absorption study of the outer Milky Way—the galaxy for which we have the best data—of Dickey et al. (2009) showed that the mean spin temperature of the atomic hydrogen is nearly constant out to 25 kpc in radius, implying that the mix of cool and warm gas is similarly independent of both radius and height above the disk.[11] Roughly 15%–20% of the gas is in the cool phase, while the rest is warm. This implies that changes in the interstellar environment (in particular, the drop in average ISM pressure) with R and z-height do not result in the disappearance of the cool phase. Both the cool and warm gases have scale heights that increase with radius. Strasser et al. (2007) showed that the distribution of the cool gas in the outer Galaxy is not random, but is preferentially found in large, coherent structures that may be connected to the Galaxy's spiral arms, suggesting that it may be gravitational perturbations that trigger the cooling of the cool atomic gas out of the warm neutral medium (WNM).

To study the detailed structure of the Milky Way's H I, Kalberla et al. (2016) combined data from the Galactic Effelsberg–Bonn H I survey with the third release of the Parkes Galactic All Sky Survey and, using an unsharp masking technique, found an abundance of small-scale cold filaments that they argue show the cold neutral medium (CNM) is largely organized in sheets that are themselves embedded within a WNM with approximately 10 times the column density of the CNM sheets ($N_{\rm H} \sim 10^{19}$ cm^{-2}); sheets, rather than clumps, are expected when pressure effects dominate over self-gravity. To what extent the outer H I disk of the Milky Way resembles the outer disk of a galaxy such as NGC 3198 is an open question.

Even in an otherwise smooth distribution, the introduction of clumpiness into the gas distribution can have a dramatic impact on the resulting radial H I distribution in the CIB photoionization model. In what follows, we include a very simple prescription for clumping of the gas in the photoionization model and show how this can lead to extended disks at much lower column densities than in the unclumped models.

3. Disk Ionization Model

3.1. Introduction

We summarize the framework of Maloney (1993) and Dove & Shull (1994) before introducing some modifications necessary for this work. The work concentrates on the $L_\star$ galaxies NGC 3198 and NGC 2997 as they share key properties with the Milky Way (Maloney 1993; Pisano 2014). They also share essentially identical distance moduli, placing them at about the same distance (Tully et al. 2016). The Cosmicflows-3 catalog gives a distance modulus for NGC 3198 of 30.61 ± 0.17 using both Cepheid variables and the Tully–Fisher relation; for NGC 2997, the Tully–Fisher distance modulus is for group member ESO 434-34 of 30.74 ± 0.40 in close proximity. From their respective rotation curves, NGC 3198 is less massive than NGC 2997 by a small factor, although their different inclinations (edge-on versus face-on) make the factor uncertain. We ignore this difference below as the corrected scale height will involve an even smaller factor. For continuity with Maloney (1993) and Dove & Shull (1994), we assume both galaxies have the same radial scaling at a distance of 9.4 Mpc. *This scaling is 40% smaller than implied by the new distance modulus from Cosmicflows-3. Thus there is a case for increasing all quoted radii throughout the paper by the same amount.* But we refrain from such a large correction to maintain continuity with the earlier work.

Both galaxies show gas disks that extend far beyond the optical emission. In NGC 3198, as discussed above, based on VLA observations, after a fairly smooth decline, the disk appears to truncate (somewhat unevenly between the two sides of the major axis) at radii between 33 and 40 kpc, where the projected column density $N_{\rm H} \sim 5 \times 10^{19}$ cm^{-2}; note that, corrected for the galaxy's substantial inclination ($i \approx 72°$), this is a face-on column density $N_{\rm H} \sim 2 \times 10^{19}$ cm^{-2}. In NGC 2997, which is at low inclination and hence geometric corrections are small, the disk extends much farther out, to approximately 53 kpc at the $N_{\rm H} \sim 1.2 \times 10^{18}$ cm^{-2} level, and any steepening in the slope of $N_{\rm H}$ versus radius occurs at or beyond the limits of the data.

Our model is based on the original observations of NGC 3198 (Maloney 1993), although we extend the work to a discussion of both NGC 2997 and the Galaxy. The galactic disk is modeled as having a spherical dark matter halo and exponential stellar + gas disk. Azimuthal symmetry is assumed, thus restricting the problem to two dimensions in (R, Z), where R denotes galactocentric radius and Z the vertical height from the midplane. Due to symmetry about the midplane, the problem can be further restricted to $Z \geqslant 0$. *We scale up the projected measures (e.g., Hα surface brightness) for two-sided photoionization.* For the gas column densities relevant to the outermost H I disk, the disk opacity is negligible for the expected metallicities.

[11] A similar conclusion was reached by Curran et al. (2016) for their sample of galaxies, which showed no evidence for radial variations in spin temperature over the inner $R \sim 30$ kpc of the galactic disks.

3.2. Galactic Model

In our ionization model, the disk is divided into a series of radial (annular) bins 1 kpc apart, going outward from the galactic center. If these radial bins are insulated against radiation emitted by neighboring bins, then the problem is reduced to a one-dimensional problem in Z at any radius R. The mass column density of stellar matter at a given radius is given by

$$\Sigma_\star(R) = \Sigma_\star(0)\exp\left(-\frac{R}{R_\star}\right)\mathrm{g\ cm^{-2}}, \quad (3)$$

where $R_\star$ is the disk scale length, which we take to be 2.7 kpc, in line with the earlier work. The column density of gas at a radius R is given by

$$\Sigma_{\rm gas} = \Sigma_0(1 + 4y)\exp\left(-\frac{R}{R_0}\right)\mathrm{g\ cm^{-2}}, \quad (4)$$

where y is the abundance of helium relative to hydrogen and the gas scale length is $R_0 = 8.8$ kpc (Maloney 1993). Note that $R_\star$ and R_0 are broadly consistent with the Galaxy (see above). The dark matter halo has a density given by

$$\rho_{dm}(Z) = \frac{\rho_{dm,0}}{1 + (R^2 + Z^2)/a^2}, \quad (5)$$

where a is the core radius (=7.92 kpc) and $\rho_{dm,0}$ (=$6.7 \times 10^{-3}\,M_\odot$ pc^{-3}) is the density at the galaxy's center (Dove & Shull 1994).

The galactic model is also explored for a disk with different filling factors f to account for a nonuniform density within each column; this increases the local density and makes the gas more difficult to ionize. We concentrate on $f = (0.01, 0.1, 1)$, which covers the range of reasonable atomic hydrogen densities[12] ($\langle n_{\rm H}\rangle = 0.1$–$10\ \mathrm{cm^{-3}}$). Because the possible ways of implementing such a volume filling factor are practically unconstrained, and because our main focus is on illustrating the effects of such clumpiness, we have chosen an extremely simple form for f.

We also explore the impact of a nonuniform covering fraction of gas c such that $c < 1$ indicates there are holes in the gas disk when viewed face-on. Clumpiness is seen in simulations of the outermost reaches of H I disks (e.g., Stewart et al. 2011). The covering fraction is a 2D (projected) quantity; the factors f and c can both be operating simultaneously and are entirely independent in our treatment. Thus, for $c < 1$, we do not attempt to conserve the gas mass at each radius. The necessary modifications are given in the next section.

3.3. Vertical Gas Distribution

The column density of H I gas at a radius R is given by Equation (4). The equation is highly idealized and may not describe the typical galaxy in detail. For example, in the Galaxy, a double exponential is needed to trace the gas (e.g., Kalberla & Dedes 2008). But our model is simple because it is grossly modified by the external radiation field.

In our calculation, we wish to find the mass density of gas ρ at a given height Z. Since the local disk potential in the outer disk is dominated by the dark matter, this is given by the equation of hydrostatic equilibrium

$$\sigma_{zz}^2\frac{\partial\rho(Z)}{\partial Z} = -\rho(Z)K_z, \quad (6)$$

where σ_{zz} refers to the vertical velocity dispersion ($\lesssim$10 km s^{-1}) and K_z the acceleration due to gravity, coupled with Poisson's equation

$$\frac{dK_z}{dZ} = -4\pi G\rho'(Z), \quad (7)$$

assuming isothermality of the disk at $T = 10^4$ K. Again, this is only a working approximation because other poorly constrained sources (e.g., magnetic fields, cosmic rays) may contribute (Cox 2005). The density ρ' now represents the local mass density in toto (stars, gas, dark matter). For our 1D calculation, we include the filling factor by decreasing the calculated gas scale height by f ($f \leqslant 1$). This compresses the gas distribution, raising the midplane density by a factor of $1/f$. This simplified treatment is intended only to illustrate how increasing the local gas densities from the smooth case will affect the truncation and extent of the disk.

A more sophisticated analysis would be to treat radiation transfer in 3D through a porous (fractal) medium (e.g., Bland-Hawthorn et al. 2015). Such a framework would be much more realistic, but it also introduces a level of poorly constrained complexity that is not justified for the presently available data. We return to this point in Section 6.

In our adopted simple form, the change in the critical column density in the presence of a volume filling factor f can be accounted for by inserting f in the numerator of Equations (1) and (2) so that N_c scales like $f^{1/2}$. Two models were used: a constant fill fraction f for all R, and a linear model in which $c = 1$ below a given cutoff radius and then decreases linearly to its minimum value at $R_{\rm max}$. The idea of a clumpy medium may appear to be inconsistent with Equations (6) and (7), but here we assume that the clumpy medium is confined by a diffuse phase transparent to radiation with negligible mass.

3.4. Radiation Field

The specific intensity of the isotropic extragalactic radiation field is assumed to obey a simple power law:

$$J_\nu = J_o\left(\frac{\nu}{\nu_o}\right)^{-\alpha}, \quad (8)$$

where ν_o is the frequency of the Lyman limit, J_o is the specific intensity of radiation (in erg cm^{-2} s^{-1} Hz^{-1} sr^{-1}) at the Lyman limit, and $\alpha \approx 1$ for a spectrum dominated by the active galactic nucleus (AGN).

4. Computational Method

Gas layers. Our method closely follows the approach of Dove & Shull (1994). For a given R, the vertical gas density profile is computed as follows. First, an initial estimate for the midplane density ρ_0 is assumed. This is used in a fourth-order Runge–Kutta routine to find $\rho(Z)$ and K_z using Equations (6) and (7); $\rho(Z)$ is then integrated over Z to find the column density. This procedure is iterated until the column density converges to that found using Equation (4). This method is used to divide the disk into a number of layers in Z, where each layer has a constant gas density. We decided on $m = 60$ layers

[12] The use of $\langle\rangle$ denotes volume-averaged densities, which are less than local densities if $f < 1$; all other density variables refer to local densities.

as this was found to yield sufficient accuracy; fewer layers led to stochastic variations at high $N_{\rm H}$.

4.1. Photoionization and Recombination Equilibrium

Photoionization and recombination equilibrium is satisfied when the number of ionizations is equal to the number of recombinations per unit volume per unit time. For an optically thick hydrogen nebula, this is given by (Osterbrock & Ferland 2006)

$$n_{\rm H\,I}\int_{\nu_0}^{\infty}\frac{4\pi J_\nu}{h\nu}\sigma_\nu d\nu = n_e n_p \alpha^B_{\rm H\,I}(T), \quad (9)$$

where J_ν is the angle-averaged specific intensity of incident radiation, σ_ν is the frequency-dependent photoionization cross-sectional area of hydrogen, and $\alpha^B_{\rm H\,I}$ is the recombination coefficient of hydrogen in an optically thick medium. This equilibrium is more generally expressed by the following equality between photoionization and recombination rates:

$$X_{i,j}\Gamma_{ij} = n_e X_{i,j\,+\,1}\alpha_{ij}(T), \quad (10)$$

where $X_{i,j}$ is the fraction of species i in ionization state j, α_{ij} is the Case A recombination rate coefficient for electron captures into the jth ionization state, and Γ_{ij} denotes the total ionization rate for species i into state $j+1$, given by

$$\Gamma_{ij} = \int_{\nu_{ij,0}}^{\infty}\frac{4\pi J_\nu}{h\nu}\sigma_{\nu,ij}d\nu + \Gamma_i^{\rm sec}, \quad (11)$$

where, for species i in ionization state j, $\sigma_{\nu,ij}$ is the photoionization cross-sectional area, and $\nu_{ij,0}$ is the minimum frequency of a photon that can ionize the species. Here, $\Gamma_i^{\rm sec}$ refers to the ionization rate of secondary ionizations, which are those resulting from high-energy electrons ionizing neutral hydrogen. However, this component is negligible and can be ignored for the given electron temperature of $T_e = 10^4$ K (Dove & Shull 1994).

There are two sources of ionization in the galactic disk—a *direct* and a *diffuse* component. The direct component refers to that from the isotropic cosmic background, and the diffuse component refers to the photons emitted by recombinations, namely those with sufficient energy to ionize hydrogen.

Direct component. The direct component resulting from the isotropic cosmic background radiation, $J_\nu^{\rm dir}$, at a layer in the disk is given by

$$J_\nu^{\rm dir} = \frac{1}{2}\int_{-1}^{0} I_\nu e^{\tau_\nu/\mu}d\mu, \quad (12)$$

where τ_ν is the optical depth between the layer and the point at which the radiation enters the disk, and μ is the cosine of the angle between the normal to the layer and the line of propagation into the layer (Maloney 1993). We have assumed that there are no additional sources of radiation in the extreme outer disk.

Diffuse component. After Maloney (1993), the diffuse mean specific intensity incident on one layer due to another layer, at height Z, an optical depth τ_ν away, $J_\nu^{\rm diff}$, is given by

$$J_\nu^{\rm diff} = \frac{1}{2}S_\nu(Z)\int_0^1 [e^{-\tau_\nu/\mu} - e^{-(d\tau_\nu+\tau_\nu)/\mu}]d\mu, \quad (13)$$

where τ_ν is the optical depth between the layers and $d\tau_\nu$ is the optical thickness of the source layer at Z. Here, $S_\nu(Z)$ is the source function at height Z, simply given by the recombination rate

$$S_\nu(Z) = n_e n_{i,j}\alpha_{ij}(T)\ {\rm phot\ cm^{-2}\ s^{-1}}. \quad (14)$$

The total rate of photoionization is influenced by both Equations (12) and (13). However, as they are interdependent —linked by electron density—an iterative scheme is required to numerically compute the final ionization fractions in each layer. Taking into account the different species present in the galactic model, the total electron density is

$$n_e = n_{\rm H\,II} + n_{\rm He\,II} + 2n_{\rm He\,III}. \quad (15)$$

Therefore, the resulting fraction of an ionized species is given by

$$\frac{X_{i,j\,+\,1}}{X_{i,j}} = (n_e\alpha_{ij}(T_e))^{-1}\int_{\nu_{ij}}^{\infty}\frac{4\pi J_\nu}{h\nu}\sigma_{\nu,ij}\,d\nu, \quad (16)$$

where $J_\nu = J_\nu^{\rm diff} + J_\nu^{\rm dir}$.

The computational method comprises two phases: the initial calculation of the ionization state from the direct radiation component only, using the "on-the-spot" approximation to treat the effect of recombinations (e.g., Osterbrock & Ferland 2006), followed by a more accurate iterative equilibrium computation.

After Maloney (1993), there are several sources contributing to the diffuse intensity $J_\nu^{\rm diff}$. These include

1. ground-state recombinations of H I, He II, and He III;
2. the $2^3S \rightarrow 1^1S$ (19.8 eV) and $2^1P \rightarrow 1^1S$ (21.3 eV) resonance-line transitions of helium;
3. the $2^1S \rightarrow 1^1S$ (two photons, combined energy 20.6 eV) transition of He I;
4. the $2^2P \rightarrow 1^2S$ (40.7 eV) Lyα He II transition;
5. He II Balmer-continuum emissions ($E \geqslant 13.6$ eV);
6. the $2^2S \rightarrow 1^2S$ (two photons, combined energy 40.7 eV) transition of He II.

Case A recombination coefficients are used in this step, as it is no longer assumed that all recombinations produce photons that are absorbed locally, and so ground-state recombinations must be considered in calculations (Osterbrock & Ferland 2006).

An initial guess is taken for the hydrogen column density at a given radius R and is used to compute a new value until the two converge, giving the final value. For each of the diffuse-radiation-producing processes, the following routine is carried out, beginning with initial guesses for species densities. First, the photoionization cross-sectional area is calculated. Optical depths for the relevant frequency are calculated using $d\tau_\nu = \sigma_{ij}n_{i,j}\Delta l$, l denoting layer height, which are then used to find the recombination rate in each layer using Equation (14), using the previously calculated species densities. Then the diffuse radiation resulting from this process incident on each layer, including contributions from all other layers in the disk (including those on the other side of the midplane), is calculated using Equation (13).

After this has been carried out for each process, the resulting diffuse radiation intensity values are used in Equation (16) to compute the ionization fraction of the species in each layer. H II, He II, and He III number and column densities can then be computed. The whole process is repeated using these as new starting values, until the values converge to no more than a

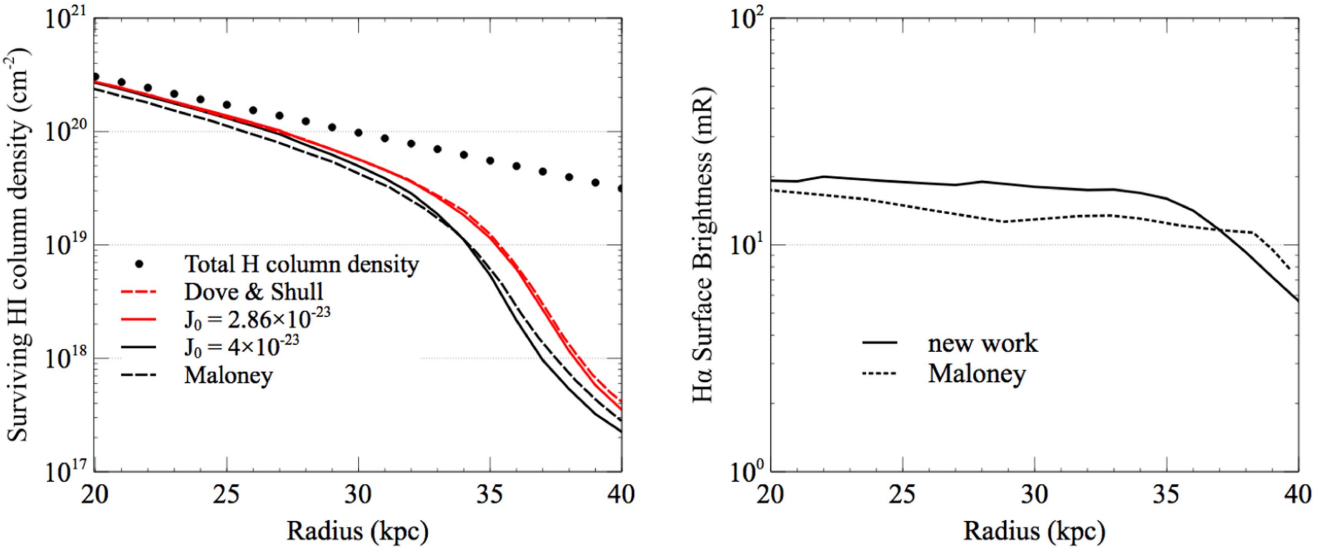

Figure 1. Left: our computed curve of the dependence of column density $N_{\rm H}$ with galactic radius (solid red line) for comparison with Dove & Shull (1994; dashed red line); we show the same comparison with Maloney (1993; dashed black line) and our model (solid black line). The adopted values of J_o (in units of erg cm^{-2} s^{-1} Hz^{-1} sr^{-1}) are chosen to match the respective values used by the above authors. The dots indicate an exponential profile for the neutral hydrogen emission in NGC 3198 prior to external photoionization. The profile is shown over the limited radial range of 20 kpc to 40 kpc, as first presented by the above authors. The gas filling fraction and covering fraction are everywhere $f = 1$ and $c = 1$, respectively. Right: our computed Hα surface brightness E_m as a function of galactic radius from a face-on disk (solid line) for comparison with Maloney (1993; dotted); this was not computed by Dove & Shull (1994).

10^{-3} discrepancy. The final electron density is used to calculate the emission measure $fn_e^2\,\Delta l$, where n_e is the electron density in each of m layers, Δl is the layer height, and f is the filling factor. This process is repeated for each radial block.

4.2. Emission Measure

An emission measure is a useful physical quantity for relating the ionizing photon flux to the induced Hα surface brightness. It has a long history in atmospheric physics and low-surface-brightness astronomical observations; for an extended discussion, see Tepper-Garcia et al. (2015). This quantity is calculated at each radial value using the simple formula for an ionized nebula taken from Spitzer (1978),

$$E_m(H\alpha) = \int_0^L n_e n_p dl \ {\rm cm}^{-6}\ {\rm pc}, \qquad (17)$$

effectively giving the sum of the total H recombinations along the line of sight L where n_p is the proton number density. For a plasma at temperature 10^4 K, an emission measure of 1 cm^{-6} pc is equivalent to an Hα surface brightness $\mu({\rm H}\alpha) = 330$ mR.

4.3. Comparison with Earlier Work

In Figure 1, we show our computed radial variation in $N_{\rm H}$ and μ(Hα) with earlier work. Our computational method is closer to that of Dove & Shull (1994), and thus the agreement for $N_{\rm H}$ is excellent when using the same cosmic ionizing intensity. These authors do not compute the trend in E_m or equivalently μ(Hα). When we rescale the CIB upward to match Maloney (1993), the agreement is not as good for the run of $N_{\rm H}$ but is sufficient for our purposes; the same holds for the trend in μ(Hα).

5. Results

In relatively isolated or loose-group spiral galaxies, the H I disk typically extends 1.5–2 times farther than the optical radius ($\mu_V = 25$ mag arcsec^{-2}) at a limiting column density of $N_{\rm H} \sim 10^{20}$ cm^{-2}; for a recent review, see Bosma (2016). These outer regions can be complicated by warps and flares, or even asymmetries induced by the galaxy's motion with respect to the local medium (e.g., Heald et al. 2016). We have ignored these details and concentrated on the survival of cool gas in the presence of an external radiation field.

Our interest has been kindled by recent discoveries of low column H I gas at very large radius from the parent galaxy (Pisano 2014; Wang et al. 2016). One of the more spectacular examples is seen in the outskirts of M31, which exhibits a collection of H I clouds at a radius of ~90 kpc in the direction of M33. The clouds have sizes of order 1 kpc and masses of order $10^5 M_\odot$ observed at H I column densities below 10^{18} cm^{-2}. For the Galaxy, Kalberla & Dedes (2008) fit the H I column density profile with a double exponential function that extends to at least 60 kpc down to $N_{\rm H} \approx 10^{18}$ cm^{-2}. In comparison, other large galaxies like M83 have huge H I disks that extend beyond 80 kpc in radius at a 10× higher column density limit of 10^{19} cm^{-2} (Koribalski 2017). At present, one can only wonder just how far this gas extends at lower column density. Our new work is intended to motivate the community to explore this tantalizing question.

We add a further note of caution: our predicted radial profiles for the H I column density ($N_{\rm H}$) and the expected Hα surface brightness (μ(Hα)) assume a smooth, face-on spiral disk. Observed profiles are normally "boosted" by the effects of disk inclination. *For smooth, diffuse emission, the observed profiles must be deprojected before a direct comparison can be made with our models (see below).* If the emission is patchy, the situation is more complex and will require a more careful treatment.

Derived column densities. In Figures 2 and 4, we revisit the calculations of Maloney (1993) and Dove & Shull (1994) over a much larger radial range. We also consider the geometric filling and covering factors f and c, which allow us to examine the impact of clumpy gas in a consistent and controlled manner.

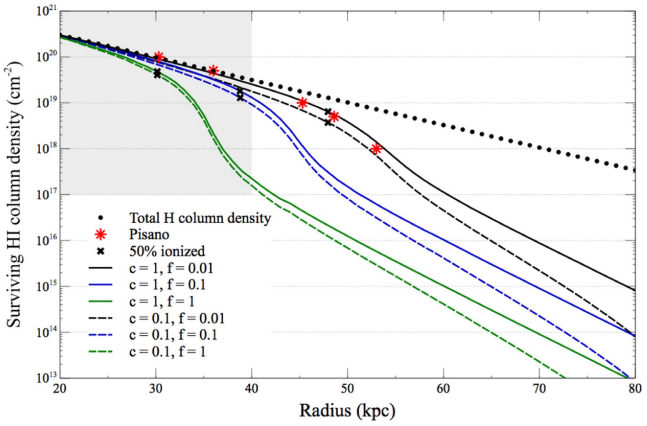

Figure 2. Impact of different filling factors (f) and covering fractions (c) on the survival of neutral gas in the presence of external photoionization. The external ionizing field is the same as in Figure 1 with J_o taken from Maloney (1993). The red asterisks are from Pisano (2014), and the black crosses indicate where the total H I column is 50% ionized. The solid and dashed curves (black, blue, green) correspond to $f = 0.01$, 0.1, 1, respectively, as indicated. The dashed lines have matching fill factors but show the trend in decreasing covering fraction, from $c = 1$ at 20 kpc to $c = 0.1$ at 80 kpc. Higher values of f increase the local gas density and make it more robust against being fully ionized. The black dots and green solid curve are the same as in Figure 1, as shown by the shaded region; note that the radial scale is increased *threefold*. For guidance, H I column densities down to $\sim 10^{16}$ cm^{-2} can be detected in emission using radio receivers; QSO absorption lines reach down to much lower columns. The gray box shows the domain of the original study by Maloney (1993) in Figure 1.

As the local density rises through decreasing f, the gas is more able to survive photoionization at a fixed J_o through faster recombination. The smallest fill factor we consider is $f = 0.01$, as this produces clouds with densities at the upper range expected in outer disks ($\sim$10 H atoms cm^{-3}).

It is important to note that there is *still* a critical column density present in all of the models: it has simply moved to lower column densities (and hence to larger radii) as a consequence of the filling factor; there is also a secondary effect of the transition getting shallower with decreasing f.

As discussed in Maloney (1993), the gas in NGC 3198 truncates at a radius of about 33 kpc to the northeast. This behavior follows the $c = 1, f = 1$ (solid green) track closely in Figure 2 ($J = J_o$). But such a cut-off is much less evident on the opposite side of the galaxy, where the gas extends (nonmonotonically) to 40 kpc. As discussed above, this may simply be a consequence of modest asymmetries in the total hydrogen distribution within the disk, which are common in spiral disks and are not terribly surprising at large radii. Another possibility is that the asymmetry is the result of differences not just in total column density but in the degree of clumpiness of the atomic gas between the two extremes of the major axis.

Alternatively, it is possible the H I disk is shaped at least partly by some other process, such as ram pressure (although NGC 3198 is notably isolated, and the asymmetries of the disk are quite modest). The northeast side may be confined by an external medium; the southwest side may represent the outer gas becoming clumpy. This type of strong to mild asymmetric ram pressure confinement of the outer H I disk is seen in dozens of nearby disks, including NGC 7421 (Ryder et al. 1997), NGC 2276 (Gruendl et al. 1993), the Large Magellanic Cloud (Kim et al. 2003; Salem et al. 2015), and in the highly inclined Sculptor galaxy NGC 253 (Koribalski et al. 1995).

If Hα emission is detected beyond an H I edge defined at some limiting column density (see Figure 3), this provides a crucial constraint on the state of the outermost gas, whether ram pressure confined or ionized by the CIB. We discuss the importance of Hα emission in more detail below.

Pisano (2014) does not provide direct information (e.g., major axis cuts) of the radial H I distribution in NGC 2997 because of the low resolution of the GBT observations. However, his Table 1 provides the extent (area) of the H I disk as a function of column density. We have used these data to derive the red points plotted in Figure 2; in effect, this is the symmetrized radial H I distribution for the modestly asymmetric disk. The plotted data match very well with the $c = 1$, $f = 0.01$ model. We note that at some level this agreement is fortuitous: the mass model used has not been matched to the rotation curve of NGC 2997 (although the effects, assuming a flat rotation curve in this region, will be modest), and we have not attempted to match the H I distribution at smaller radii. We note also that the large beam of the GBT means that the inner disk is not well resolved. However, it does demonstrate that such a model can easily explain the extent of the disk and the slow roll-off of the neutral hydrogen. Now consider Figure 4, where we present the same model parameters for a weaker cosmic ionizing intensity ($J = 0.1J_o$) at the low end of the likely CIB intensity. Again fortuitously, the red points fall along the $c = 1$, $f = 0.1$ (solid blue) track. This demonstrates the strong degeneracy between J and f. As the models show, there is a degeneracy between J, f, and c.

In our simple model for NGC 3198 (Figure 2), the H I column densities are (10^{20}, 10^{19}, 10^{18}, 10^{17}, 10^{16}) cm^{-2} at (30, 50, 70, 90, 110) kpc before photoionization by the CIB. After imposing a high value of J_o, the crossing points plummet to (27, 34, 37, 42, 51) kpc (see Table 1). But for a gas-rich system with a covering fraction of unity, the filling factor has a major impact on the extent of the detectable H I gas. Even for our strongest external radiation field, the crossing points move out to (29, 46, 54, 61, 70) kpc for the case $f = 0.01$. The 50% ionization radius now occurs at $r_{0.5} = 48$ kpc; that is, the neutral extent of the disk has more than doubled in area. The crossing points for all models are presented in Table 1.

In Figure 4, we consider a weak external field, with $J = 0.1J_o$. For $f = 1$, the crossing points are now approximately (29, 41, 46, 51, 60) kpc as a function of the column density. For our lowest f value, these move out to (30, 49, 61, 69, 79) kpc. The 50% ionization radius now occurs at $r_{0.5} = 58$ kpc such that we may expect to find detectable H I gas *twice* as far out as indicated by the early NGC 3198 data, at least in principle.

For all models, the columnar ionization fraction is increasing with radius. In the last row of Table 1, we list the radius at which the total column of hydrogen becomes 50% ionized. As indicated, the 50% ionization radius for Maloney (1993) is $r_{0.5} \approx 30$ kpc at a column density of H I above $10^{19.5}$ cm^{-2}. For all other models, $r_{0.5}$ occurs at lower $N_{\rm H}$ and is up to a factor of two farther out in the most extreme cases.

A broad distribution in f is a natural consequence of a turbulent medium (Lazarian & Pogosyan 2000). A spread in c can arise from increased clumping of the outer disk gas as the cold-flow accretion channel becomes more dispersed, as observed in numerical simulations (Nuza et al. 2014; Scannapieco et al. 2015; Crain et al. 2017). Thus we consider the effect of a slowly declining covering fraction, as shown by the dashed lines

Table 1
H I Column Density as a Function of Galactic Radius R (kpc) for Different Combinations of J, f, c

$\log N_{\rm H}$ ($\rm cm^{-2}$)	R (kpc)											
	$J = J_o$						$J = 0.1J_o$					
	$c = 1$ $f = 1$	$c = 0.1$ $f = 1$	$c = 1$ $f = 0.1$	$c = 0.1$ $f = 0.1$	$c = 1$ $f = 0.01$	$c = 0.1$ $f = 0.01$	$c = 1$ $f = 1$	$c = 0.1$ $f = 1$	$c = 1$ $f = 0.1$	$c = 0.1$ $f = 0.1$	$c = 1$ $f = 0.01$	$c = 0.1$ $f = 0.01$
16	50.9	48.7	60.2	56.9	69.5	64.9	60.2	56.9	69.5	64.9	78.8	72.4
16.5	46.5	44.8	55.5	53.0	64.8	61.1	55.5	53.0	64.8	61.1	74.0	68.7
17	42.3	41.2	51.3	49.5	60.5	57.7	51.3	49.5	60.5	57.7	69.4	65.2
17.5	39.1	38.5	47.9	46.8	56.8	54.9	47.9	46.8	56.8	54.9	65.1	61.7
18	37.0	36.7	45.6	44.8	53.9	52.2	45.6	44.8	53.9	52.2	61.0	57.4
18.5	35.7	35.4	43.7	42.8	50.7	48.6	43.7	42.8	50.7	48.6	55.7	51.8
19	34.2	33.8	40.9	39.7	45.8	43.3	40.9	39.7	45.8	43.3	48.5	44.9
19.5	31.7	31.1	36.1	34.7	38.5	36.4	36.1	34.7	38.5	36.4	39.4	37.0
20	26.7	26.1	28.5	27.7	29.4	28.2	28.6	27.7	29.4	28.3	29.7	28.5
50% ionized	**30.1**	30.1	38.8	38.8	48.0	48.0	38.8	38.8	48.0	48.0	57.8	57.8

Note. Column 8: $(J, f, c) = (J_o, 1, 1)$ is the original model first presented by Maloney (1993). The columnar ionization fraction for all models increases with radius. The last line indicates the radius ($r_{0.5}$), which corresponds to 50% ionization of the total hydrogen column. The 50% cut-off radius of Maloney (1993) is bolded to emphasize the radial extent of all other models.

in Figures 2 and 4. As expected, a correction for a decreasing covering fraction shortens the crossing-point distances.

Patchy gas makes detection more difficult generally. This can lead to both a lower covering fraction within the telescope beam and a complex line profile in velocity space. Simply stated, a covering fraction of c requires a telescope with an aperture that is $1/c$ times larger to observe the same signal under the same observing conditions. The deepest H I observations require the largest apertures if the gas fills or partially fills the beam. But if the gas is in the form of dense "nuggets," higher sensitivity can be achieved by resolving out the clumps, for example, using spectroscopy with a very long baseline interferometer (VLBI).

Derived emission measures. In Figures 3 and 5, we also present the predicted Hα surface brightnesses for the strong and weak external fields, respectively. The boosted signal from clumping, if relevant, is included in the predictions. For the maximum cosmic intensity, we expect 20 mR at best, declining to a few milli-Rayleigh (mR) at the limit of the data; for the weak external field, the expected value is an order of magnitude less. As already mentioned, an Hα surface brightness of 1 mR is exceedingly faint, corresponding to 5.7×10^{-21} erg $\rm cm^{-2}$ $\rm s^{-1}$ $\rm arcsec^{-2}$ in more conventional units (Bland-Hawthorn et al. 1995). This level of sensitivity is an order of magnitude fainter than what is possible in conventional spectroscopy and needs some explanation. There are two approaches: the first averages over most or all of the detector to achieve the detection limit, and the second results from stacking many independent spectra.

Bland-Hawthorn et al. (1997) use Fabry–Perot "staring," where the detector is azimuthally binned to produce a narrow spectroscopic band (~10 Å). Apertures are typically in the range of 5 arcmin to 1 degree (e.g., Madsen et al. 2001). The smaller apertures are well matched to the resolution of the biggest single-dish radio telescopes. Zhang et al. (2016) use a very different method. They identify 0.5 million galaxies with 7 million sight-line spectra, which are coadded once shifted to a laboratory rest frame. They detect the presence of emission-line gas out to 100 kpc and identify this as being primarily from the hot halo. In reality, a substantial contribution may come from an extended thick disk.

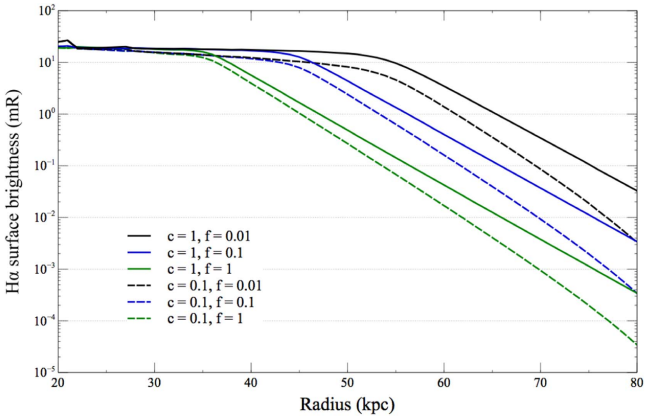

Figure 3. Predicted Hα surface brightness for the models presented in Figure 2 where the disk is seen face-on. The calculation is for two-sided ionization given that the cosmic ionizing intensity illuminates both sides of the H I disk; the internal dust extinction is assumed to be negligible, as expected in the outer parts of galaxies. For a disk inclined with angle i (where $i = 0$ is face-on), the predicted values should be increased by $\sec i$ for $i < 90°$; see text for a full discussion on this correction. For guidance, an Hα surface brightness below 1 mR is currently undetectable.

In principle, it is possible to boost the projected signal from the cosmic ionizing intensity. The one-sided ionizing photon rate (phot $\rm cm^{-2}$ $\rm s^{-1}$) is given by

$$\phi_i = \pi \int_{\nu_o}^{\infty} \frac{J_\nu}{h\nu}\, d\nu, \tag{18}$$

where the cosmic ionizing spectrum J_ν is defined in Equation (8). This reduces to $J_o = \alpha h \phi_i / \pi$, which establishes a simple relationship between ϕ_i and J_o, both of which can be related easily to the Hα surface brightness μ:

$$\mu(\mathrm{H}\alpha) = 4.5\mathcal{G}\left(\frac{\phi_i}{10^4 \text{ phot } \rm cm^{-2}\ s^{-1}}\right) \quad \mathrm{mR}, \tag{19}$$

assuming the H I slab of gas is optically thick to UV radiation (Bland-Hawthorn & Maloney 1999). In fact, we can do better than this, as indicated by the geometric factor $\mathcal{G}$. Weymann et al. (2001) note that the high inclination i of a flat structure of

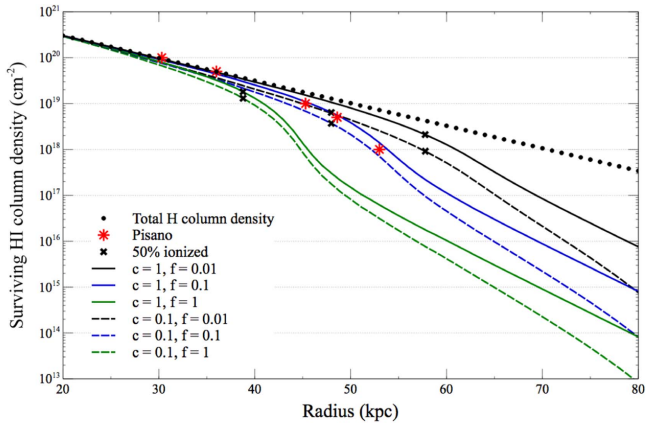

Figure 4. The impact of different filling factors (f) and covering fractions (c) on the survival of neutral gas in the presence of external photoionization. The external ionizing field is now $J = 0.1J_o$, i.e., 10% of the assumed cosmic intensity in Figure 2. The solid curves correspond to $f = 0.01$, 0.1, 1 as indicated. The dashed lines have matching filling factors but show the trend in decreasing covering fraction, from $c = 1$ at 20 kpc to $c = 0.1$ at 80 kpc. Higher values of f increase the local gas density and make it more robust against being fully ionized.

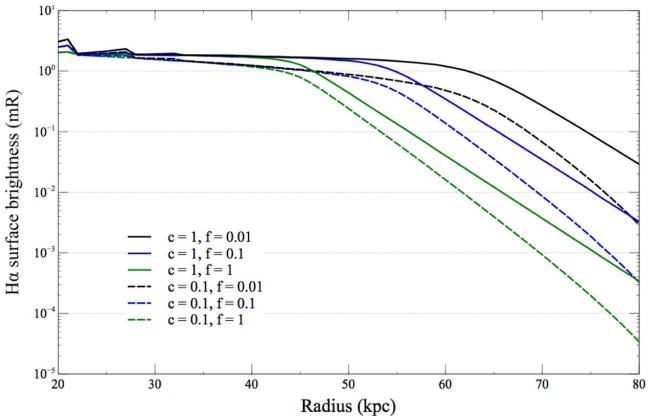

Figure 5. The predicted Hα surface brightness for the models presented in Figure 4 where the disk is seen face-on. The calculation is for two-sided ionization given that the cosmic ionizing intensity illuminates both sides of the H I disk; the internal dust extinction is assumed to be negligible, as expected in the outer parts of galaxies. For a disk inclined with angle i (where $i = 0$ is face-on), the predicted values should be increased by $\sec i$ for $i \lesssim 90°$. For guidance, an Hα surface brightness below a few milli-Rayleigh is currently undetectable.

gas (H I 1225+01) can be exploited because of the increased path length through its ionized outer surface. There is an additional factor of two from the gas sheet being ionized on both sides. Thus, under certain circumstances, we can boost the observed signal in Equation (19) by $\mathcal{G} = 2/\cos i$. This factor cannot increase indefinitely and is likely to break down for angles steeper than about $i = 70°$–$75°$. The $\mathcal{G}$ values for NGC 3198 ($i = 72°$) and NGC 2997 ($i = 30°$) are $\lesssim$5.9 and 2.3, respectively. This method allowed Weymann to set the deepest outer disk upper limit to date: 8 mR (2σ). A higher deprojected upper limit of about 20 mR was established from null detections in the extreme outer disk of M31 (Madsen et al. 2001; Adams et al. 2011).

For individual galaxies, the deepest outer disk detection is from Bland-Hawthorn et al. (1997). These signals at 50–100 mR are surprisingly strong, even after considering geometric corrections, and reflect either the presence of star formation activity at exceedingly low levels or the warp of the outer disk causing the gas to be exposed to the inner radiation field, that is, self-ionization (Bland-Hawthorn 1998). Interestingly, there is new evidence of very weak star formation in the outer warped disk of one disk galaxy, which makes it possible to age-date the onset of the warp (Radburn-Smith et al. 2014). Such activity may be affecting outer disk measurements in other galaxies (Christlein et al. 2010; Fumagalli et al. 2017).

The recent claim of a roughly 20 mR indirect detection of the CIB in the outer disk of UGC 3721 is not obviously consistent with the nondetections mentioned above, especially the Weymann et al. (2001) result, even with due consideration for patchy emission or deprojection (Fumagalli et al. 2017). The deepest nondetection experiments were undertaken with Fabry–Perot in "staring" mode (Bland-Hawthorn et al. 1994, 1995). In principle, the much larger $\mathcal{R}\Omega$ product of a Fabry–Perot interferometer, where $\mathcal{R}$ is the spectral resolving power and Ω is the instrument solid angle, makes it far more sensitive to diffuse light than conventional spectrographs.

However, the Fumagalli result is consistent with estimates for the CIB intensity based on the low-redshift Lyα forest and the most recent theoretical estimates of the background, as discussed in the Introduction. Given these disparate results, caution in interpreting current measurements is mandatory, but as we discuss in the next section, there is some prospect of a more definitive detection.

6. In Search of the Outer Disk Material

Faint Hα *emission.* So what are the prospects for detecting this outer protodisk material in spatially resolved imaging or spectroscopy? We stress that detailed models will be needed to associate the beam-smoothed H I and Hα measurements discussed here with the intrinsically much higher spatial resolution observations from QSO absorption-line measurements.

The predicted emission measures for the warm ionized gas are likely to be too low for most galaxy environs, as we have shown. Even in the most advantageous situations, we need stacking over many galaxies or the Fabry–Perot "staring" technique, which washes out the structure. Encouragingly, in the past few years, the first detections of emission from warm gas in the circumgalactic environment ($R \sim 100$ kpc) have been made. In all cases, the surface brightness is exceedingly faint, requiring long integration times, data stacking, or areal binning in observations with our most advanced telescopes. Zhang et al. (2016) detect Hα+[NII] emission at exceedingly faint levels ($\sim$3 mR) in the 50–100 kpc radius bin in 7 million stacked spectra from the SDSS survey. This is an order of magnitude fainter than the levels observed by Bland-Hawthorn et al. (1997) and Christlein et al. (2010) in their survey of Hα emission at or beyond the H I edge of nearby galaxies, although the detection limit of the former method is of order 1 mR at 1σ (Bland-Hawthorn et al. 1994; Madsen et al. 2001).

The Dragonfly technique (van Dokkum et al. 2014) of using many Canon cameras with their near-perfect antireflection coatings is worth pursuing, but this approach is hampered by the need for a narrowband ($\lesssim$10Å) filter. These cannot be installed in the fast camera beam (Bland-Hawthorn et al. 2001)

Table 2
Fields of View (FoV), Angular and Spatial Resolutions, 1σ H I Column Densities (N_H), H I Mass Sensitivities, and Survey Speeds (SS) for Different Telescopes Based on a Total Integration Time of 100 hr

Telescope	FoV$_\eta$ deg^2	Res. (arcsec)	Res. ($(D/10$ Mpc) kpc)	N_H (cm^{-2} 20 km s^{-1})	Mass ($(D/10$ Mpc$)^2$ $M_\odot$)	SS	SS$_{N_H}$
SKA-MID[a]	0.43	29	1.4	1.5e17	5.0e3	1.0e-4	0.085
MeerKAT[a]	0.66	30	1.4	4.1e17	1.5e4	1.7e-5	0.015
ASKAP[a]	24	21	1.0	8.8e18	1.6e5	5.4e-5	0.0024
JVLA-C[a]	0.16	25	1.2	2.7e18	6.5e4	4.8e-6	0.003
JVLA-D[a]	0.16	83	4.0	2.5e17	6.5e4	4.8e-6	0.033
FAST[b]	0.021	180	8.5	2.1e16	1.4e4	5.3e-6	0.17
GBT[c]	0.01	550	27	2e16	1.3e5	4.7e-8	0.014
Survey							
HALOGAS[d] (WSRT)	0.16	40	2.0	2.5e18	8.5e4	⋯	⋯
IMAGINE[e] (ATCA)	0.20	140	7.0	2.4e17	1.0e5	⋯	⋯
MHONGOOSE[f](MeerKAT)	0.66	30	1.4	1.2e18	4.8e4	⋯	⋯
MHONGOOSE[f] (MeerKAT)	0.66	90	3.5	1.3e17	4.8e4	⋯	⋯

Notes. For all telescopes, this is the time to map an area the size of the SKA-MID FoV (0.43 deg^2), or larger if indicated. All physical quantities are scaled to a distance of 10 Mpc.
[a] Based on Popping et al. (2015).
[b] Nan et al. (2011).
[c] Extrapolated from Wolfe et al. (2016).
[d] Heald et al. 2010.
[e] http://imagine-survey.org
[f] http://mhongoose.astron.nl

and instead must be inserted at the entrance aperture of the telescope.[13]

In order to exclude faint starlight, the resultant images must be compared with broadband images using a red filter presumably from a companion Dragonfly system. The combined signal could reasonably get down to a few milli-Rayleigh smoothed over a 10″ patch of sky for one or more fields in several dark nights. This is the sensitivity needed if we are to detect the ionized layer in the protodisk region. Our estimate comes from the 3σ broadband (B, I) limit (30 mag arcsec^{-2}) of the Dragonfly system. Here we assume this performance holds for the R band. For background-limited observations (sky+galaxy continuum), an emission-line region with a surface brightness of 500 mR detected within the band ($\Delta\lambda_R \approx 140$ nm) is detected with the same sensitivity. If we replace the R filter with a 100× narrower bandpass filter, as in the UKST experiment, our detection limit falls to 50 mR. We get another factor of 10 gain (5 mR at 3σ) by smoothing the diffuse data over a 10″ patch. Our wild extrapolations assume the instrument response (e.g., flat-fielding) can be removed to better than 0.1% or so (Bland-Hawthorn et al. 1994, 1995).

Faint HI emission. If the goal is to "image" the protodisk region, we argue here that the best prospect is to go after the clumpy, cool gas emission. Support for this idea comes from the simulations of Nuza et al. (2014), where clumpy H I gas is "observed" to occupy a complex, roughly planar network of filaments—we refer to this scree of material as the *protodisk region*. Their simulations are broadly tuned to the characteristics of the Local Group. The cool protodisks for M31 and the Galaxy are seen to overlap and to extend out to at least 100 kpc from both galaxies.[14]

Interestingly, Wolfe et al. (2013, 2016) imaged an area of 12 square degrees mapping the region between M31 and M33 with a 5σ detection level of $N_H = 3.9 \times 10^{17}$ cm^{-2} over 30 km s^{-1} and found discrete clouds that have a typical size of a few kiloparsecs and a H I mass of $10^5\,M_\odot$. Upcoming observations of nearby galaxies will achieve this sensitivity or better (Table 2). Popping et al. (2009) gave detection limits for a number of telescopes including ASKAP and the SKA using the best sensitivity estimates at the time. Here we expand this table with better sensitivity predictions and include contemporary surveys as a point of reference.

Popping et al. (2015) have made detailed performance simulations of the SKA and SKA precursors based on the actual baseline configuration and telescope design. We use their methods to derive new sensitivity estimates based on the latest specifications as currently presented by the SKA office. In Table 2, we present 1σ column densities and H I mass sensitivities for a number of different facilities. The mass estimates come from assuming the limiting column density is uniform across the beam. In order to compare the performance of different radio telescopes, both interferometers and single-dish telescopes, we make certain assumptions. In our analysis, we assume that the area imaged corresponds to a field of view of 0.43 deg^2 if the quoted field is smaller than this solid angle. This is chosen as it is equivalent to the field of view of SKA-MID, which sets the benchmark for future studies. Single-dish telescopes can only observe a single pointing equivalent to their angular resolution, and therefore we take into account the

[13] This method was used successfully by Parker & Bland-Hawthorn (1995) for the UK Schmidt Hα survey with an entrance Hα filter (10 Å FWHM) 14 inches in diameter. The crude optics and detector system meant that the detection limit was $\gtrsim$300 mR.

[14] In a comment on this work, K.C. Freeman posed an interesting question as to whether the filamentary H I networks in groups like Leo and M81, long assumed to be tidal debris from outer disk interactions, are more likely to arise from interlocking protodisk regions. The distinction here is that the outer disks are only now forming for the first time.

number of pointings that are required to map the same solid angle.

As our aim is to search for low-column-density H I gas around galaxies, we assume an observation time of 100 hr per object. This integration time is typical for these kind of studies, for example, HALOGAS on WSRT (Heald et al. 2010), IMAGINE on ATCA (http://imagine-survey.org), and MHONGOOSE on MeerKAT (http://mhongoose.astron.nl). The angular resolution of interferometers is dependent on the baseline distribution and moderated by the weighting and tapering of the visibility data. In order to make a fair comparison, we use the natural resolution of each interferometer—without using any weighting—as this gives the highest flux sensitivity and represents the resolution that is best matched to the baseline distribution. In Table 2, the columns and cloud masses are ideal for targets like NGC 3198 and NGC 2997. The tabulated numbers are scaled to a distance of 10 Mpc for consistency with both galaxies.

To understand which radio telescope is best for mapping an extended area that is larger than a single pointing, we calculate the survey speed defined as $\mathrm{SS} = \mathrm{FoV}_\eta/\mathrm{rms}^2/t_{\mathrm{int}}$, where FoV_η is the effective field of view and t_{int} is the integration time. The effective field of view represents the noise equivalent area of the beam and is given by $\mathrm{FoV}_\eta = (\pi/8)(1.3\lambda/D)^2$. The survey speed is relevant when concentrating on the flux sensitivity, but becomes meaningless for the surface brightness, which depends on the (synthesized) beam area. To encapsulate this difference, we define a surface brightness survey speed as $\mathrm{SS}_{N_{\mathrm{H}}} = (\mathrm{FoV}_\eta \cdot b_{\mathrm{maj}} \cdot b_{\mathrm{min}})/\mathrm{rms}^2/t_{\mathrm{int}}$. For interferometers, we calculate the flux and brightness sensitivities without any tapering of the visibility data and using natural weighting (no down-weighting of data). This will give the best flux sensitivity at the natural resolution. The synthesized beam of an interferometer can be altered by weighting of the UV data, which can greatly enhance the surface brightness sensitivity. For ASKAP and FAST, the effective field of view is larger than a single beam due to the phased array feed on ASKAP and the 19-multibeam on FAST. The extraordinary potential of the recently commissioned FAST telescope is clear. Another powerful approach is H I absorption-line spectroscopy, which favors interferometers observing bright background sources. This experiment will be addressed in future work.

Combined H I *and* Hα *studies.* As we have discussed, there is a degeneracy between the intensity of the CIB and the total hydrogen distribution that produces an observed neutral hydrogen distribution. This also depends on the degree of clumping of the gas and on the gas covering factor. One way to break this degeneracy is through simultaneous measurements of both the H I and Hα emission. For a smooth gas distribution, this is discussed in detail by Fumagalli et al. (2017), who used the combination of the H I profile with their measured Hα flux to derive their constraints on the CIB.

Detailed mapping of both the neutral and ionized emission potentially offers a powerful probe of both the CIB intensity and the neutral gas column density distribution and the degree of clumping; provided that the same gas dominates both the H I and Hα emission, any patchiness of the disk emission will drop out. We have not discussed such models for two main reasons: (1) It would be very premature. At present, the needed data sets simply do not exist, and although we have suggested ways in which they might be obtained—and for H I emission, the needed facilities either are now or will soon be available–at the moment, increasing the complexity of the models cannot be justified. Note that the detailed modeling carried out by Fumagalli to constrain the CIB assumed a smooth distribution of gas and essentially was based on just two observed quantities, the location of the ionization front (what we refer to in this paper as the truncation radius) and the surface brightness of the Hα emission interior to the truncation radius. (2) For a clumpy disk, it is not only necessary to adopt a 3D treatment of the radiative transfer but assumptions also need to be made about the gas clumpiness as a function of radius and height above the plane. Even in the Milky Way, these are not well-determined quantities, and hence model parameters that are poorly constrained would be introduced. What should drive this type of modeling would be the discovery from high-S/N (signal-to-noise ratio) data sets (at minimum, well-resolved radial profiles of both the H I and Hα emission) that no reasonable smooth models were capable of simultaneously fitting both the H I and Hα data.

7. Discussion

Outer disk regions remain mysterious. Most disk galaxies appear to be warped and often flared in the outermost parts, at least in H I (Briggs 1990). Another recent revelation is that the declining metallicity gradient of both stars and gas appears to flatten out beyond several disk scale lengths (Vlajić 2010; Sanchez et al. 2014). It is interesting to consider whether some of the extended H I envelopes identified in nearby groups (e.g., Leo, Cen, M81, M83) normally attributed to tidal debris from high column regions is in fact compressed material from protodisk regions. How can we distinguish between these cases? This is something that future simulations might address.

But it remains unclear how many scale lengths in radius we need to explore to establish clear evidence of cool flows from the intergalactic medium. Just how the metal-poor gas arrives, and in what state, is a topic of debate. With reference to the QSO absorption-line work, are we seeing halo gas, a disk–halo transition region, or cooling material settling into an outer "protodisk"? Curran et al. (2016), combining data from a number of surveys and incorporating upper limits, found the first evidence for an anticorrelation between H I 21 cm absorption strength and impact parameter in galaxies. This suggests that there may be a condensation process at work in which the galactic interstellar medium (ISM) condenses from the CGM, which in turn is accreted from the intergalactic medium.

Borthakur et al. (2016) studied the ISM–CGM relation in a sample of H I-detected galaxies from the GASS survey whose circumgalactic media were probed via COS Lyα absorption in the spectra of background quasars with impact parameters in the range 60–230 kpc. Roughly 90% of the galaxies showed Lyα absorption, and there was a strong correlation between the galaxy atomic gas mass fraction ($M_{\mathrm{H\,I}}/M_*$) and the impact-parameter-corrected Lyα equivalent width, suggesting a physical connection between the atomic ISM and the CGM; that is, the H I disks are being fueled by accretion from the CGM. Studies of the kinematics of low-redshift Mg II absorbers, from modeling of line profiles, suggest a combination of disk rotation plus radial infall or radial inflow (Charlton & Churchill 1998; Ho et al. 2017).

Arguably the most tantalizing evidence for some kind of accretion flow comes from the outer reaches of redshifted

galaxies probed by quasar sight lines (e.g., Charlton & Churchill 1998; for a recent review, see Ho et al. 2017). The Mg II absorption doublet in the UV has long been known to trace the H I gas down to $N_{\rm H} \sim 10^{17}\,{\rm cm}^{-2}$ in disk galaxies, that is, gas that is optically thick at the Lyman limit (Bergeron & Stasińska 1986; Steidel et al. 2002).

From an extensive literature review, a "typical" redshifted disk galaxy produces the following absorption signatures: damped Lyα ($R \lesssim 15$ kpc); Mg II ($R \lesssim 100$ kpc); O VI ($R \lesssim 200$ kpc). The damped Lyα limit is from Charlton & Churchill (1998), the Mg II limit is from Ho et al. (2017), and the O VI limit is from Kacprzak et al. (2015). The radial limits scale statistically with a number of other factors: (1) the galaxy's K-band luminosity (Steidel et al. 1995); (2) the cosmic ionizing intensity: at lower redshift, Mg II can be traced to larger radius because the ionizing intensity is weaker (Bergeron et al. 1994).

The trend in recent papers is to ascribe some of the action in QSO sight lines to a spherical outflow (Nielsen et al. 2017), particularly at high redshift. The observed epoch is critical: what we infer during the golden age of star formation and AGN activity ($z = 1$–5) does not necessarily follow for all time. In contrast to the strong, kinematically broadened structure at earlier times, coplanar gas is clearly seen in the weak absorbers (Kacprzak & Churchill 2011; Kacprzak et al. 2011; Matejek et al. 2013; Kacprzak et al. 2015; Ho et al. 2017).

Tumlinson et al. (2013) provide a census of the neutral hydrogen absorption in the halos of a sample of 44 low-redshift ($z \sim 0.2$) $L \sim L_\star$ galaxies with the Cosmic Origins Spectrograph on *HST*, in which the QSO sight line passes within 150 kpc of the galaxy (the COS-Halo sample). Of most relevance to this paper, they find (1) strong H I absorption in the circumgalactic media of their sample galaxies, (2) that this absorption arises at velocities indicating that the absorbing material is bound to the galaxies, and (3) this absorption arises in gas at temperatures much lower than the virial temperature, indicating that the gas has either cooled and condensed subsequent to shock-heating or was never heated to the virial temperature. A comparison with other samples of Lyα absorption indicates that there is an increase in the strength of Lyα absorption within an impact parameter of ~200 kpc, consistent with the kinematic association of the absorption with the galaxies in the COS-Halo sample.

In principle, these data could be used to constrain the column density distributions we discuss here. However, in practice there are difficulties, some of which Tumlinson et al. discuss in their own comparison with galactic disks (their Section 6.3.1). Foremost among these is the very large uncertainty in the COS-Halo H I column densities over the range at which they would provide the most constraints. Due to saturation of the line profiles, all of the COS-Halo measurements within an impact parameter of 70 kpc are lower limits (aside from one damped Lyα system), with the caveat that the column densities are probably below $N_{\rm H} \approx 10^{18-18.5}\,{\rm cm}^{-2}$, due to the absence of damping wings in the line profiles. Hence all of the COS-Halo $N_{\rm H}$ columns have one to three orders of magnitude uncertainty over the precise range of impact parameter (20–70 kpc) in which measurements would be most useful.

What we can say is that the Tumlinson results are inconsistent with a model in which their QSO sight lines intercept disks such as we model here if the areal filling factor is close to unity at $R \sim 40$ kpc and below. Given the very small number of galaxies with impact parameters this small in their sample, this is not so surprising (see also their comparison with the Kalberla & Dedes Milky Way disk model). We note that areal filling factors of 0.3–0.5 quoted in their paper have a modest impact on beam-averaged emission models compared to their effects on absorption statistics.

Binney (1992) concluded in a review on outer disks that "one's best guess must be that warps *will* in the end prove to be valuable probes of cosmic infall and galaxy formation." Ultimately, there *must* be a coplanar "protodisk" region if we are to account for the thinness of disks (Matthews, et al. 1999), their exponential profiles (Mestel 1963; Fall & Efstathiou 1980), and their outer warps (Briggs 1990; Binney 1992). Some have suggested that this coplanar region is the likely site of inflow accretion (e.g., Kacprzak et al. 2015), but clear kinematic evidence of this is hard to come by at present. The spatially resolved structure and extent of this protodisk region are unknown. The numerical simulations (e.g., Popping et al. 2009; Nuza et al. 2014; Scannapieco et al. 2015) are fairly rudimentary at this stage and need to include more microphysics and higher spatial resolution before convergence is achieved across different hydrodynamical codes (Kereš et al. 2012).

We have made a case that, under favorable conditions, the protodisk region may be directly detectable in emission. Powerful radio facilities (Table 2) are coming on line that can directly tackle this question, and we urge telescope allocation committees to embrace the unknown. New facilities should always be pushed to their limits; short time allocations rarely break new ground. If successful, this would herald a new era in tracing how disk galaxies are fed by the intergalactic medium.

J.B.H. is supported by a Laureate Fellowship from the Australian Research Council. A.S. is supported under this grant. A.Z. was supported by J.B.H.'s earlier Federation Fellowship from the Australian Research Council. J.B.H. acknowledges insightful conversations with Ken Freeman, Bärbel Koribalski, and Jacqueline van Gorkom over two decades on the nature of the outer disks of spirals. We are grateful to Yuval Birnboim, Naomi McClure-Griffiths, Jay Lockman, John Dickey, and Ron Ekers for continued inspiration in this wonderfully rich and underappreciated field. We are indebted to an inspired referee for their deep insight and assistance.

ORCID iDs

Joss Bland-Hawthorn https://orcid.org/0000-0001-7516-4016
Attila Popping https://orcid.org/0000-0001-9234-1088

References

Abramova, O. V. 2012, AstL, 38, 222
Adams, J. J., Uson, J. M., Hill, G. J., & MacQueen, P. J. 2011, ApJ, 728, 107
Anderson, M. E., & Bregman, J. N. 2011, ApJ, 737, 22
Bergeron, J., & Stasińska, G. 1986, A&A, 169, 1
Bergeron, J., Petitjean, P., Sargent, W. L. W., et al. 1994, ApJ, 436, 33
Binney, J. J. 1992, ARA&A, 30, 51
Birnboim, Y., & Dekel, A. 2003, MNRAS, 345, 349
Bland-Hawthorn, J., Ekers, R. D., van Breugel, W., Koekemoer, A., & Taylor, K. 1995, ApJL, 447, L77
Bland-Hawthorn, J., Freeman, K. C., & Quinn, P. J. 1997, ApJ, 490, 143
Bland-Hawthorn, J., & Maloney, P. R. 1999, ApJL, 510, L33
Bland-Hawthorn, J., Sutherland, R., & Webster, D. 2015, ApJ, 807, 154

Bland-Hawthorn, J., Taylor, K., Veilleux, S., & Shopbell, P. L. 1994, ApJL, 437, L95
Bland-Hawthorn, J., van Breugel, W., Gillingham, P. R., Baldry, I. K., & Jones, D. H. 2001, ApJ, 563, 611
Bland-Hawthorn, J. 1998, Galactic Halos, 136, 113
Bochkarev, N. G., & Sunyaev, R. 1977, SvA, 21, 542
Borthakur, S., Heckman, T., Tumlinson, J., et al. 2016, ApJ, 833, 259
Bosma, A. 2016, in Astrophysics and Space Science Library, Vol. 434, Outskirts of Galaxies, ed. J. H. Knapen, J. C. Lee, & A. Gil de Paz (Berlin: Springer), 209
Braun, R., & Thilker, D. A. 2004, A&A, 417, 421
Briggs, F. 1990, ApJ, 352, 15
Charlton, J. C., & Churchill, C. W. 1998, ApJ, 499, 181
Christlein, D., Zaritsky, D., & Bland-Hawthorn, J. 2010, MNRAS, 405, 2549
Ćirković, M. M., Bland-Hawthorn, J., & Samurović, S. 1999, MNRAS, 306, L15
Codis, S., Pichon, C., & Pogosyan, D. 2015, MNRAS, 452, 3369
Corbelli, E., & Salpeter, E. E. 1993, ApJ, 419, 104
Cornuault, N., Lehnert, M., Boulanger, F., & Guillard, P. 2016, A&A, in press (arXiv:1609.04405)
Cox, D. P. 2005, ARA&A, 43, 337
Crain, R. A., Bahć, Yannick M., Lagos, C. del P., et al. 2017, MNRAS, 464, 4204
Curran, S. J., Reeves, S. N., Allison, J. R., & Sadler, E. M. 2016, MNRAS, 459, 413
Dai, X., Anderson, M. E., Bregman, J. N., & Miller, J. M. 2012, ApJ, 755, 107
Dickey, J. M., Strasser, S., Gaensler, B. M., et al. 2009, ApJ, 693, 1250
Dove, J. B., & Shull, J. M. 1994, ApJ, 423, 196
Dubois, Y., Pichon, C., Welker, C., et al. 2014, MNRAS, 444, 1453
Faerman, Y., Sternberg, A., & McKee, C. F. 2017, ApJ, 835, 52
Fall, S. M., & Efstathiou, G. 1980, MNRAS, 193, 189
Felton, J. E., & Bergeron, J. 1969, ApL, 4, 155
Fumagalli, M., Haardt, F., Theuns, T., et al. 2017, MNRAS, in press (arXiv:1702.04726)
Gruendl, R. A., Vogel, S. N., Davis, D. S., & Mulchaey, J. S. 1993, ApJL, 413, L81
Haardt, F., & Madau, P. 2012, ApJ, 746, 125
Heald, G., Józsa, G. I. G., Serra, P., et al. 2010, in AIP Conf. Proc. 1240, Hunting for the Dark: The Hidden Side of Galaxy formation, ed. V. P. Debattista & C. C. Popescu, (Melville, NY: AIP), 164
Heald, G., de Blok, W. J. G., Lucero, D., et al. 2016, MNRAS, 462, 1238
Ho, S. H., Martin, C., Kacprzak, G., & Churchill, C. 2017, ApJ, 835, 267
Kacprzak, G. G., & Churchill, C. W. 2011, ApJL, 743, L34
Kacprzak, G. G., Churchill, C. W., Evans, J. L., Murphy, M. T., & Steidel, C. C. 2011, MNRAS, 416, 3118
Kacprzak, G. G., Muzahid, S., Churchill, C. W., Nielsen, N. M., & Charlton, J. C. 2015, ApJ, 815, 22
Kalberla, P. M. W., & Dedes, L. 2008, A&A, 487, 951
Kalberla, P. M. W., Kerp, J., Haud, U., et al. 2016, ApJ, 821, 117
Kereš, D., & Hernquist, L. E. 2009, ApJL, 700, L1
Kereš, D., Katz, N., Fardal, M., Davé, R., & Weinberg, D. H. 2009, MNRAS, 395, 160
Kereš, D., Katz, N., Weinberg, D. H., & Davé, R. 2005, MNRAS, 363, 2
Kereš, D., Vogelsberger, M., Sijacki, D., Springel, V., & Hernquist, L. 2012, MNRAS, 425, 2027
Khaire, V., & Srianand, R. 2015, MNRAS, 451, L30
Kim, S., Staveley-Smith, L., Dopita, M. A., et al. 2003, ApJS, 148, 473
Kollmeier, J. A., Weinberg, D. H., Oppenheimer, B. D., et al. 2014, ApJL, 789, L32
Koribalski, B., Whiteoak, J. B., & Houghton, S. 1995, PASA, 12, 20
Koribalski, B. 2017, in IAU Symp. 321, Formation and Evolution of Galaxy Outskirts, ed. B. L. Ziegler et al. (Cambridge: Cambridge Univ. Press), 232
Lazarian, A., & Pogosyan, D. 2000, ApJ, 537, 720
Madau, P., & Haardt, F. 2015, ApJL, 813, L8
Madsen, G. J., Reynolds, R. J., Haffner, L. M., Tufte, S. L., & Maloney, P. R. 2001, ApJL, 560, L135
Maloney, P. 1993, ApJ, 414, 41
Maloney, P. R., & Bland-Hawthorn, J. 1999, ApJL, 522, L81
Maloney, P. R., & Bland-Hawthorn, J. 2001, ApJL, 553, L129
Matejek, M. S., Simcoe, R. A., Cooksey, K. L., & Seyffert, E. N. 2013, ApJ, 764, 9
Matthews, L. D., Gallagher, J. S., & van Driel, W. 1999, AJ, 118, 2751
Mestel, L. 1963, MNRAS, 126, 553
Miller, M. J., & Bregman, J. N. 2013, ApJ, 770, 118
Mo, H. J., Mao, S., & White, S. D. M. 1998, MNRAS, 295, 319
Nan, R., Li, D., Jin, C., et al. 2011, IJMPD, 20, 989
Nielsen, N. M., Kacprzak, G. G., Muzahid, S., et al. 2017, ApJ, 834, 148
Nuza, S. E., Parisi, F., Scannapieco, C., et al. 2014, MNRAS, 441, 2593
Oosterloo, T. A., Morganti, R., Sadler, E. M., van der Hulst, T., & Serra, P. 2007, A&A, 465, 787
Osterbrock, D. E., & Ferland, G. J. (ed.) 2006, Astrophysics of Gaseous Nebulae and Active Galactic Nuclei (2nd ed.; Sausalito, CA: Univ. Science Books)
Parker, Q. A., & Bland-Hawthorn, J. 1995, PASA, 15, 33
Pisano, D. J. 2014, AJ, 147, 48
Popping, A., Davé, R., Braun, R., & Oppenheimer, B. 2009, A&A, 504, 15
Popping, A., Meyer, M., Staveley-Smith, L., et al. 2015, in Proc. Advancing Astrophysics with the Square Kilometre Array (AASKA14), 132, http://pos.sissa.it/cgi-bin/reader/conf.cgi?confid=215
Radburn-Smith, D. J., de Jong, R. S., Streich, D., et al. 2014, ApJ, 780, 105
Ryder, S. D., Purcell, G., Davis, D., & Andersen, V. 1997, PASA, 14, 81
Salem, M., Besla, G., Bryan, G., et al. 2015, ApJ, 815, 77
Sanchez, S., Sánchez, S. F., Rosales-Ortega, F. F., Iglesias-Páramo, J., et al., et al. 2014, A&A, 563, 49
Scannapieco, C., Creasey, P., Nuza, S. E., et al. 2015, A&A, 577, A3
Shull, J. M., Moloney, J., Danforth, C. W., & Tilton, E. M. 2015, ApJ, 811, 3
Spitzer, L. 1978, Physical Processes in the Interstellar Medium (New York: Wiley)
Steidel, C. C., Kollmeier, J. A., Shapley, A. E., et al. 2002, ApJ, 570, 526
Steidel, C. C., Pettini, M., & Hamilton, D. 1995, AJ, 110, 2519
Stewart, K. R., Kaufmann, T., Bullock, J. S., et al. 2011, ApJ, 738, 39
Strasser, S. T., Dickey, J. M., Taylor, A. R., et al. 2007, AJ, 134, 2252
Sunyaev, R. A. 1969, ApL, 3, 33
Tepper-Garcia, T., & Bland-Hawthorn, J. 2017, MNRAS, in press
Tepper-Garcia, T., Bland-Hawthorn, J., & Sutherland, R. 2015, ApJ, 813, 94
Tully, R. B., Courtois, H. M., & Sorce, J. G. 2016, AJ, 152, 50
Tumlinson, J., Thom, C., Werk, J. K., et al., et al. 2013, ApJ, 777, 59
van Dokkum, P. G., Abraham, R., & Merritt, A. 2014, ApJL, 782, L24
van Gorkom, J. 1991, in ASP Conf. Ser. 16, Atoms Ions and Molecules: New Results in Spectral Line Astrophysics, ed. A. D. Haschick & P. T. P. Ho (San Francisco, CA: ASP), 1
Viel, M., Haehnelt, M. G., Bolton, J. S., et al. 2017, MNRAS, 467, L86
Vlajić, M. 2010, PASA, 27, 252
Walsh, W., Staveley-Smith, L., & Oosterloo, T. 1997, AJ, 113, 1591
Wang, J., Koribalski, B. S., Serra, P., et al. 2016, MNRAS, 460, 2143
Westmeier, T., Braun, R., & Thilker, D. 2005, A&A, 436, 101
Westmeier, T., Koribalski, B. S., & Braun, R. 2013, MNRAS, 434, 3511
Weymann, R. J., Vogel, S. N., Veilleux, S., & Epps, H. W. 2001, ApJ, 561, 559
Wolfe, S. A., Lockman, F. J., & Pisano, D. J. 2016, ApJ, 816, 81
Wolfe, S. A., Pisano, D. J., Lockman, F. J., McGaugh, S. S., & Shaya, E. J. 2013, Natur, 497, 224
Zhang, H., Zaritsky, D., Zhu, G., Ménard, B., & Hogg, D. W. 2016, ApJ, 833, 276